

Journal of Materials Chemistry A

Accepted Manuscript



This is an *Accepted Manuscript*, which has been through the Royal Society of Chemistry peer review process and has been accepted for publication.

Accepted Manuscripts are published online shortly after acceptance, before technical editing, formatting and proof reading. Using this free service, authors can make their results available to the community, in citable form, before we publish the edited article. We will replace this *Accepted Manuscript* with the edited and formatted *Advance Article* as soon as it is available.

You can find more information about *Accepted Manuscripts* in the [Information for Authors](#).

Please note that technical editing may introduce minor changes to the text and/or graphics, which may alter content. The journal's standard [Terms & Conditions](#) and the [Ethical guidelines](#) still apply. In no event shall the Royal Society of Chemistry be held responsible for any errors or omissions in this *Accepted Manuscript* or any consequences arising from the use of any information it contains.

Electrodeposition and pyrolysis of Mn/polypyrrole nanocomposites: a study based on soft X ray absorption, fluorescence and photoelectron microspectroscopies

Benedetto Bozzini^{1*}, Patrizia Bocchetta¹, Belén Alemán², Matteo Amati², Alessandra Gianoncelli², Luca Gregoratti², Hikmet Sezen², Antonietta Taurino³ and Maya Kiskinova²

¹Dipartimento di Ingegneria dell'Innovazione, Università del Salento, via Monteroni, 73100 Lecce, Italy

²Elettra – Sincrotrone Trieste SCpA, SS14-Km163.5 in Area Science Park, 34149 Trieste, Italy

³Institute for Microelectronics and Microsystems, IMM-CNR, via Monteroni, 73100 Lecce, Italy

*corresponding author: benedetto.bozzini@unisalento.it

ABSTRACT

Electrodeposition of manganese/polypyrrole (Mn/PPy) nanocomposites has been recently shown to be a technologically-relevant synthesis method for the fabrication of Oxygen Reduction Reaction (ORR) electrocatalysis. In this study we have grown such composites with a potentiostatic anodic/cathodic pulse-plating procedure and characterised them by a multi-technique approach, combining a suite of in situ and ex situ spectroscopic methods with electrochemical measurements. We have thus achieved a sound degree of molecular-level understanding of the hybrid co-electrodeposition process consisting in the electropolymerisation of polypyrrole with incorporation of Mn. By in situ Raman we followed the formation of MnO_x and polymer by monitoring the build-up and development of the relevant vibrational bands. The compositional and chemical-state distribution of the as-deposited material has been investigated ex situ by soft X-ray fluorescence (XRF) mapping and micro-absorption spectroscopy (micro-XAS). XRF shows that the spatial distribution of Mn is consistent in a rather wide range of current densities (c.d.), while micro-XAS reveals a mixture of Mn valencies, with higher oxidation states prevailing at higher c.d.s. The pyrolysis of the electrodeposits, desirable for obtaining more durable and active catalysts, has been followed in situ by photoelectron microspectroscopy, allowing to assess the evolution of: (i) the electrodeposit morphology, resulting in a uniform distribution of nanoparticles; (ii) the chemical state of manganese, changing from a mixture of valences to a final state consisting of Mn(III) and Mn(IV) oxides and (iii) the bonding nature of nitrogen, from initially N-pyrrolic to a combination of pyridinic and Mn-N/graphitic.

KEYWORDS

Manganese; Polypyrrole; ORR; Electrodeposition; Nanocomposites; X-ray microscopy; SPEM

1. INTRODUCTION

The high cost and limited availability of platinum have intensified the research of novel non-noble metal catalysts for the oxygen reduction reaction (ORR). Their performance in alkaline media is particularly important for energy conversion applications, such as alkaline fuel cells¹ and metal/air batteries². Since the discovery of cobalt phthalocyanine as an active material towards ORR³ and of the beneficial effect of pyrolysis at high temperatures (400-800°C) on its stability and catalytic activity,^{4,5} considerable attention has been dedicated to the study of pyrolysed non-precious metal-nitrogen-carbon materials (M/N/C, M=Co, Fe, Mn, etc.) as prospective electrocatalysts for ORR.⁶⁻²¹ Although the mechanism leading to the modifications of the active sites during pyrolysis is still uncertain, the increased electrocatalytic activity after heating is often attributed to the formation of MeN_x-type moieties.^{6,22-25} Among the different strategies used to build nitrogen into the catalyst, electrochemistry offers the possibility of using polypyrrole (PPy) with the dual function of N-source and electronically conducting catalyst support for the electrodeposition of metal-containing materials. PPy possesses a relatively high nitrogen content and electrical conductivity²⁶ and it can be easily synthesized through anodic electrodeposition²⁷. Its excellent ability to support catalysts has been reported for the cases of metal oxides²⁸ and metal complexes^{29,30}. As far as the type of metal-containing species is concerned, we have chosen to focus on manganese dioxide, which is probably the most widely investigated cathode material for metal/air batteries, owing to its low cost and high ORR activity in alkaline solutions, resulting from its capability of decomposing hydrogen peroxide.³¹⁻³³ It is worth noting that just a few papers have dealt with composite Mn/PPy-based electrocatalysts,³⁴⁻⁴⁰ while cobalt and iron species embedded in various forms into PPy have been rather extensively studied.

At variance with the most common protocols used to fabricate MnO₂/carbon⁴¹ and metal/PPy electrocatalysts (typically: functionalisation of carbon nanoparticles by chemical polymerisation of pyrrole, followed by the chemical reduction of a metal salt, impregnated of into the polymer⁴²⁻⁴⁵),

we have studied a one-pot electrochemical route to deposit Mn/PPy onto conductive substrates, that is better suited to form Mn/N/C catalytic systems directly in the electrodeposition process. The electrochemical process is followed by pyrolysis, which drastically increases both catalytic activity^{34,42} and durability of polypyrrole-metal compounds, due to the formation of active sites favouring the four-electron transfer ORR mechanism pathway, thus reducing the peroxide generation rate.^{46,47} The notably better oxidation resistance of the graphitic support generated by pyrolysis, with respect to that of as-electrodeposited PPy, makes binary^{48,49} or ternary⁵⁰ varieties of this material attractive for application as bifunctional oxygen electrocatalysts: we have already studied the synthesis of Mn-based/PPy binaries^{36,37} and ternaries^{38,51}, the issue of bifunctional electrocatalysis will be considered in future research in our group.

The advantage of the direct electrochemical functionalisation of appropriate catalyst supports, such as carbon, with M/N/C hybrids resides in the possibility of gaining fine control over the morphological and chemical properties of the electrodeposits, resulting in potential control on activity, selectivity and durability of the catalyst.⁵² Previous work has demonstrated the possibility of co-electrodepositing PPy and metal nanoparticles from solutions containing pyrrole and a metal salt (Au⁵³, Ni⁵⁴, Fe⁵⁵). Regarding Mn, the galvanostatic anodic electrodeposition of MnO₂ into PPy has been also reported for application in electrochemical supercapacitors.⁵⁶ To the best of the authors' knowledge, only one paper deals with ORR studies at pyrolysed Mn/PPy electrocatalysts prepared by electrosynthesis³⁴ and a study aimed at the understanding the combined role of electrodeposition of the precursor and subsequent pyrolysis is still missing.

In this work, we have electrodeposited Mn/PPy nanocomposites, we have investigated in detail the morphology and chemistry of the as-plated material by XAS and XRF microspectroscopy and we have followed in situ the pyrolysis process by scanning photoelectron microscopy.

2. EXPERIMENTAL

2.1 Materials and Electrodes

Acetonitrile, $\text{MnCl}_2 \cdot 6\text{H}_2\text{O}$ and pyrrole were supplied by Aldrich. Before each electrodeposition experiment, the pyrrole monomer was distilled under rotary pump vacuum the number of times required to render it colourless (typically 3). Water used for the preparation of the solutions was obtained with a MilliQ system (resistivity: $18.2 \text{ M}\Omega \cdot \text{cm}$). The bath compositions are detailed were relevant. The electrochemical syntheses were performed using a three-electrode cell. In this study, for the different purposes detailed in the individual Sections, we employed different working electrodes (WE): glassy carbon (GC) rod ($\Phi=3\text{mm}$), graphite disk ($\Phi=10\text{mm}$), gold rod ($\Phi=5\text{mm}$) and Cu TEM grids. A Pt wire of 1.88 cm^2 was used at the counter electrode (CE). The reference electrode (RE) was an aqueous silver/silver chloride ($\text{Ag}/\text{AgCl}/3\text{M}$: $0.209 \text{ V}/\text{NHE}$) one, connected to the solution with a salt bridge; the liquid junction potential between aqueous and non-aqueous solutions has been checked to be negligible. All the potentials reported in this paper are referred to this reference scale.

2.2 Electrochemical measurements and methods

The electrochemical measurements were performed at room temperature (25°C) using a PAR VersaSTAT 4 potentiostat. Cyclic voltammetric analyses have been carried out at GC electrode in the range $-1.8 \div 1.2 \text{ V}$ at a scan rate of 0.1 V s^{-1} in de-aerated acetonitrile solutions containing 1 vol.% H_2O and 0.1M TBAP supporting electrolyte, with additions of: (i) 0.1M pyrrole; (ii) 0.05M MnCl_2 and (iii) both 0.1M pyrrole and 0.05M MnCl_2 . The choice of acetonitrile as the solvent, is dictated by the width of its electrochemical window, allowing more flexibility in the pulsed co-electrodeposition with reactive metals than water.^{35-40,57,58} Addition of small amounts of H_2O in acetonitrile baths for PPy electrodeposition, has been reported to increase the rate of pyrrole electropolymerisation owing to a reduced electrostatic repulsion among hydrated radical cations.⁵⁹

Moreover, the presence of water in acetonitrile has been proved beneficial in PPy electrodeposition for the mechanical (chiefly adhesion) and electrical (mainly electronic conductivity) properties of the polymer film; in fact, owing to its stronger basicity with respect to pyrrole, it consumes the protons liberated by the electropolymerization process, avoiding monomer protonation that brings about electrode passivation.^{60,61} Basicity is further ensured by acetonitrile hydrolysis, yielding acetic acid and NH_3 .^{62,63} Perchlorate counter-ions ensure the electronic and structural properties required for the co-electrodeposition of PPy/metal oxide composites. In fact, a crucial aspect of the composite plating of metals and conducting polymers is that the latter materials are generally doped and conducting under anodic conditions (both during electropolymerisation and in contact with electrolytes containing doping anions), while under the cathodic polarisation typical of metal electrodeposition, they undope and become insulating. This metal-to-insulator transition is commonly explained in terms of percolation between electronically conducting islands embedded in an amorphous non-conducting matrix. Such transition depends on polymer properties, among which the most significant ones seem to be: type of counter-ion, doping level and degree of structural disorder. These processes can be rationalised effectively within the semi-empirical framework of the Electrochemically Stimulated Conformational Relaxation (ESCR) model proposed in ref. [64] and therein quoted literature; briefly: anodic polarisation of a PPy film generates localised radical cations along the polymeric chains, resulting in electrostatically driven conformational changes associated with an increase of free volume. In order to ensure electroneutrality, anions are attracted into the polymeric network and their penetration is favoured by the matrix expansion. When, instead, a cathodic polarisation is applied, the polymer expels the anions and the film shrinks, eventually becoming closed and trapping the counterions that stabilise the charge carriers of the polymer backbone. Of course, undoping kinetics depends on the instantaneous diffusion coefficient that, in turn, depends on the instantaneous degree of shrinking. According to this mechanism, in principle, the choice of appropriate cathodic conditions and accurate consideration of the capacitive transients, allow to apply the reducing conditions in such a way that the required amount of metal

can be plated before the undoping transient is completed. Moreover, the progressive change of polymer electronic conductivity taking place during transient undoping can be exploited to control the relative nucleation and growth processes, offering an additional handle for particle morphology tailoring.⁵⁸ It is worth noting that MnO₂/PPy composites can be electrodeposited in a single-step one-pot anodic process from an electrolyte containing pyrrole and Mn(II),⁶⁵ nevertheless, the scope of the present investigation involves the co-electrodeposition of binary^{36,37} and ternary^{38,51} Mn-based composites and, since the elemental form of the alloying element is of interest, in this study we have concentrated on the combined anodic/cathodic process. Finally, it is worth noting that it has been shown that deep reduction of PPy can result in the stabilisation of the conductivity, probably owing to enhanced trapping of counterions by structural shrinking and closure:⁶⁶ this finding has been used for the metallisation of such deeply reduced PPy substrates, but in principle it could also find applications in the co-electrodeposition processes of interest in this study.

Nitrogen (SIAD 0.6) was bubbled for 20 min into the solution before the measurements and an N₂ blanket was kept above the solution during electrochemistry. In the case of GC, graphite and Au, the WE was polished mechanically to a mirror finish before each experiment and subsequently subjected to ultra-sonication in distilled water for 10 min and cyclic voltammetric oxidation of impurities in 0.5 M H₂SO₄ in the potential range 0÷1.5 V at a scan rate of 0.1 V s⁻¹, as recommended in ref. [34]. The CE was cleaned by immersion in concentrated HNO₃ solution to remove metal contaminations and by annealing in a butane flame to eliminate organic residues.

The Mn/PPy catalyst has been synthesized by slightly modifying a step pulsed potential procedure suggested in the literature,³⁴ consisting in suitable repetition of the cycle depicted in Figure 1 composed by an initial step at 0 V for 1 s (#1), a subsequent anodic pulse at +1.2 V for 0.5 s (#2), a cathodic step at -1.8 V for 0.5 s (#3) and a final anodic step at +1.2 V for 0.2 s (#4). The potential

values have been selected according to cyclo-voltammetric results presented and discussed in Section 3.1.1.

2.3 In situ Raman spectroscopy

Raman spectra were recorded using a LabRam microprobe confocal system. A 50× long-working distance objective was used and the excitation line at 632.8 nm was provided by a 12 mW He-Ne laser. A 600 grid/mm spectrometer was employed. The slit and pinhole were set at 200 and 400 μm, respectively, corresponding to a resolution of 2 cm⁻¹ and a scattering volume of ~3 pL. The recorded Raman intensities are directly proportional to the discharge current of the CCD detector. In situ electrochemical measurements were performed in Ventacon® glass cells with Au disc electrodes (Ø 5 mm) embedded in Teflon holders. The counter electrode was a Pt wire loop of total area ca. 2 cm², concentric and coplanar with the gold working electrode. In order to achieve Surface Enhanced Raman activity (SERS effect), the electrode was submitted to an ORC treatment consisting in cycling the electrode in a separated cell in 0.1 M KCl in the range 0.3÷1.2 V at 0.5 V s⁻¹ for 50 times.

2.4 Pyrolysis procedure

The Mn/PPy catalysts electrodeposited on graphite were subjected to pyrolysis in a tubular quartz continuous flow reactor equipped with temperature control and gas management manifold. N₂ at a flow rate of 80 cm³ min⁻¹ was used as the blanket gas. After purging with N₂ for 10 min, the temperature was increased at a rate of 10 °C min⁻¹ and then kept constant for 2 h at 670 °C. The pyrolysis process has been also performed in the SPEM analysis chamber in Ultra High Vacuum (UHV) (10⁻¹⁰ mbar): the heating rate in this case was 1°C min⁻¹.

2.5 FE-SEM

The morphology of the Mn/PPy electrodeposits was investigated by using an NVISION 40 Zeiss, equipped with a high resolution Gemini Field Emission Gun (FEG) scanning electron microscope column and with an Oxford INCA 350 Xact Energy Dispersive X-Ray Spectrometer (EDS).

2.6 SPEM

Scanning photoelectron microscopy (SPEM) measurements were performed at the ESCA-microscopy beamline of the Elettra synchrotron laboratory in Trieste, Italy. This microscope uses zone plate focusing optics providing a microprobe of diameter of ~100 nm and operates in both imaging and spectroscopy modes. Photoemission spectra of selected regions and chemical maps were acquired with 0.3 eV energy resolution by using 754 eV photon energy. More details about the microscope set-up and operation parameters can be found in ref.s [67,68].

2.7. Soft X-ray absorption and fluorescence mapping

Soft X-ray transmission microscopy (STXM), coupled with micro-spot X-ray absorption spectroscopy (XAS) and X-ray Fluorescence (XRF) elemental mapping experiments were performed at the TwinMic beamline of Elettra synchrotron facility (Trieste, Italy). Details on the technique and endstation structure can be found in ref.s [69,70].

3. RESULTS AND DISCUSSION

3.1 Electrodeposition of Mn/PPy composites

3.1.1. Cyclic voltammetry

Figure 2 reports cyclic voltammograms corresponding to: (A) pyrrole polymerisation, (B) Mn electrodeposition and (C) codeposition of polypyrrole and Mn from the solutions detailed in Section 2.2.

3.1.1.1. Electropolymerization of pyrrole - Figure 2-A shows the voltammograms for polypyrrole synthesis by application of 30 cycles in the range -2.0÷1.2 V. The initial scan of the sequence was a cathodic-going one, starting from 0.0 V. From the first cycle it appears that the electropolymerisation process begins on the polymer-free GC surface at potentials higher than 0.9 V, in agreement with literature data obtained in similar experimental conditions.³⁴ Going on with cycling, two waves appear: the first one (I) during the positive-going scan at ~ 0÷0.4 V and the second one (II) during the cathodic scan at ~ -0.2÷0.0 V, corresponding, respectively, to the doping-undoping processes of the PPy film with perchlorate anions, according to the reaction scheme Eq. (1):



The potentials at which the doping-undoping waves are found agree well with those reported in the literature for PPy doping with ClO_4^- .^{71,72}

3.1.1.2. Electrodeposition of Mn - In order to better understand the mechanism of Mn incorporation into PPy during composite electrosynthesis, the electrochemical behaviour of a pyrrole-free MnCl_2 -containing solution has been also investigated in the range -1.8÷1.2 V (Figure 2-B). Several valence states are possible for Mn in the relevant electrochemical conditions, that span both cathodic and anodic polarisations.^{73,74} As proved by in situ SPEM and Raman in a previous work of ours,⁴⁰ the

anodic polarisation of GC in Mn^{2+} containing solution at the investigated potentials can yield manganese (III, IV) oxides. Moreover, several reports exist in the literature regarding the electrodeposition of Mn(IV) oxides from aqueous Mn^{2+} -containing electrolytes in polarisation conditions similar to those employed in the present study,⁷⁵ following the overall reaction Eq. (2):



Actually, the global reaction Eq. (2) occurs via a sequence of reaction steps.^{76,77} Mn(II) ions are readily oxidised to Mn(III) ions (Eq. (3)):



and, since Mn^{3+} ions are not thermodynamically stable in neutral solutions, a disproportionation reaction occurs⁷⁷ (Eq. (4)):



Mn^{4+} then transforms into insoluble MnO_2 by reacting with water (Eq. (5)):



Another way by which MnO_2 can form, is via the electrochemical oxidation of Mn^{3+} through the MnOOH intermediate formed by hydrolysis of Mn^{3+} (Eq. (6)):



This mechanism, universally accepted for the oxidation Mn(II) salts in aqueous solution, can be considered plausible also in our acetonitrile solutions which contain a controlled amount of water.

From the inset of Figure 2-B one can notice that in the anodic-going scan of the first cycle (fresh GC surface), starting from OCP an anodic peak appears at ca. 0.6 V, followed by a Tafel-type growth at ca. 0.90 V, that can be ascribed to the multi-step process illustrated in Eq.s (3)-(6). This result agrees with the CV study of different polyimine complexes of manganese perchlorate in acetonitrile reported in ref. [78], where anodic peak potentials relating to the oxidation of Mn(II) species fall in the range 1.25÷1.36 V, depending on the nature of the complex. In the cathodic-going scan, the wave observed at ca. 1 V can be attributed to the reduction of MnO₂ to MnOOH,^{75,79} while the current onset at ca. -1.5 V indicates that reduction of Mn²⁺ to Mn(0) takes place, in agreement with literature results regarding both aqueous⁸⁰ and acetonitrile⁸¹ solutions. The large difference between the potential of this reduction peak and that of the subsequent anodic one (ca. 1 V) suggests that the electroreduction of Mn metal is an irreversible process. It is worth noting that a similar type of irreversibility has been observed in 0.066 M MnCl₂/dimethyl formamide solution with a Pt WE.⁸² It should also be noted that, according to thermodynamics in aqueous solution,⁷³ the cathodically formed Mn metal is expected to oxidise yielding Mn²⁺ at low pH or Mn(OH)₂/HMnO₂⁻ at high pH. In the subsequent scans, the two novel anodic waves appearing at ca. 0.6 and 0.7 V can be attributed to the oxidation reaction of Mn(0) and Mn(III) species formed in the previous scan. In correspondence, the new cathodic wave observed at ca. 0.3 V can be associated to the reduction of MnOOH to Mn(II) species.^{75,83}

3.1.1.3. Electrodeposition of Mn/PPy composites – In Figure 2-C we report the cyclic voltammetric curves obtained in the bath containing both pyrrole and MnCl₂. It can be noticed that the electron-transfer processes corresponding to the Mn(II)/Mn(III) reaction and to the doping of PPy run in the same potential range. Moreover, it can be observed that the reduction process of Mn(II) to Mn(0) occurring at ca. -1.5 V in the absence of pyrrole (Figure 2-B), is suppressed by the presence of the polymer. At variance with the curves obtained in the Mn²⁺ free solution (Figure 2-A), the PPy

undoping feature is less evident with respect to the doping one, indicating that the incorporation of Mn species in the polymer during the anodic scan modifies its electronic structure. The synergistic role of the co-electrodeposited metal ion in the doping-undoping process has been pinpointed, for the Mn-Co/PPy system, by in situ XAS.³⁷

The merely electrochemical analyses described in Section 3.1.1 provide useful information on the redox behaviour of Mn species, but they are insufficient to definitively establish the valence state of Mn, owing to the complex electrochemistry of the bath, the presence of several Mn complexes and concurrent redox processes. For this reason, a multi-technique approach based on micro-X ray absorption spectroscopy, X ray fluorescence mapping, photoelectron spectromicroscopy and in situ Raman spectroscopy has been adopted for the study of our Mn/PPy composites.

In order to optimise the electrodeposition conditions in view of subsequent pyrolysis, we have assessed the impact of the number of plating cycles on the structure of the pyrolysed composite. SEM morphologies of the deposits as a function of the number of deposition cycles (2, 60, 80, 120) are reported in Figure 3. By increasing the number of pulse-plating cycles the particle size increases: 51 ± 31 nm (60 cycles), 60 ± 23 nm (80 cycles), 65 ± 144 nm (120 cycles). EDX spectra collected on the particles in a large number of areas of all the samples grown in this study, confirm the presence of manganese and oxygen: a typical spectrum is overlapped to the SEM image corresponding to 60 cycles in Figure 3. No EDX signal from Mn or O could be recorded on the flat areas away from the particles. The structure corresponding to 60 cycles has been regarded as optimal and selected as the typical working condition for subsequent work: more details on this issue are provided in Section 3.3).

3.1.2. In-situ Surface-Enhanced Raman Spectroscopy (SERS) during Mn/PPy electrodeposition

In situ SERS analyses have been carried out to monitor the growth of Mn/PPy at the molecular level. In order to perform electrodeposition onto SERS-active substrates, a gold working electrode has been used, submitted to ORC treatment, as described in Section 2.3. In Figure 4 we report potential-dependent series of in situ Raman spectra recorded in baths containing only MnCl_2 (Panel (A)) and both pyrrole and MnCl_2 (Panels (B) and (C)). In Panel (A) it can be noticed that the spectral pattern recorded under OCP conditions with an ORC-treated Au electrode shows the bands at 385 and 923 cm^{-1} corresponding to C-C \equiv N bending and C-C skeletal of CH_3CN solvent.⁶³ The Raman spectra recorded during the application of a sequence of anodic potentials up to 2 V feature well-defined peaks at 253-270 and 332-346 cm^{-1} together with a set of broad bands in the range 500-750 cm^{-1} . The peaks at 253 and 270 cm^{-1} lie in the typical Raman shift range of poorly diagnostic M-O stretching and M-O-M bending vibrations^{40,84} that can be attributed to Mn (II, III, IV) oxy-hydroxides. The slight differences in Raman shift values found at different anodic potentials can be explained by the formation of different types of oligomers. In fact, the chemical equilibria leading to their formation are strongly affected by local pH and $\text{Mn}^{3+}/\text{Mn}^{4+}$ concentrations which both decrease upon anodic polarisation (see Eq.s (2) and (6b)). In addition to oxy-hydroxide bands, under the anodic conditions typically used for pulse-plating (e.g. +1.2 V), the presence of $\gamma\text{-MnO}_2$ and $\gamma\text{-Mn}_2\text{O}_3$ is also detected. In fact, the peaks at 270, 518, 657 cm^{-1} can be attributed to $\gamma\text{-MnO}_2$,⁸⁵ while the main peaks at 270 and 332-346 cm^{-1} and the broad peak centered at 657 cm^{-1} can be assigned to $\gamma\text{-Mn}_2\text{O}_3$.⁸⁶ As shown in Figure 4-A, by decreasing the electrode potential down to -2 V, the Raman features attributed to manganese oxide and/or hydroxide species disappear, indicating that their formation is associated to an electrochemical oxidation process.

In Panels (B) and (C) of Figure 4 we report potential-dependent Raman spectra recorded with the solution containing both pyrrole and MnCl_2 . The electropolymerisation of metal-free PPy from the bath of interest in this study and the modifications of the Raman bands due to the doping/undoping of the polymer have been insightfully investigated in ref. [39]. Briefly, the polypyrrole undoping

process, associated to electrochemical reduction, gives rise to a shift of the C=C stretching band from 1612 cm^{-1} , characteristic of the oxidised form, to 1569 cm^{-1} .^{87,88} Of course, the oxidation/reduction processes of PPy involve the fully reduced state (PPy⁰), the oxidized bipolaron (PPy²⁺) state and the intermediate polaron (PPy⁺) oxidized state. The bands located at about 994 and 938 cm^{-1} correspond, respectively, to bipolaron (dication) and polaron (radical cation) ring deformations,^{89,90} while the two peaks found at about 1090 and 1052 cm^{-1} can be attributed to the N-H in-plane deformation of the oxidized and reduced polypyrrole states.⁹¹

In the wavenumber range $500\text{--}750\text{ cm}^{-1}$, the Raman vibrations of Mn oxyhydroxide species cannot be detected, probably owing to the presence of overwhelming PPy bands. Nevertheless, two broad peaks at 245 and 442 cm^{-1} are found to grow with the anodic potential, that can be attributed to Mn-O and Mn-O-H bending modes as well as to Mn-N stretching. Notwithstanding the limited speciation capability of Raman in this particular case, the evident differences in vibrational properties of the Mn-related bands found in the absence and in the presence of PPy, suggest the existence of interactions between Mn and the polymer.

3.2 Characterization of as-deposited Mn/PPy composites

3.2.1. Soft X-ray absorption and fluorescence mapping

3.2.1.1 Electrodeposition set-up and current density distribution - Cu TEM grids (Figure 5-A were used for the growth of Mn/PPy composites: the grids were mounted in a hanging-meniscus configuration, ensuring a controlled c.d. distribution (c.d.d.). Both Au and Cu TEM grids were considered in preliminary work, and we found that Cu grids did not undergo appreciable corrosion during the anodic periods of the plating process. In particular, no grid distortions were recorded and EDX analyses of the electrodeposited films did not show any Cu contamination. During electrodeposition a composite film spreads from the bars, forming an ideal sample for transmission work. The polymer matrix is initially formed at the grid bars and spreads into the hollow square starting from the corners, driven by the surface tension of the growing film. During film growth, the

c.d.d. changes as the grid becomes covered with the electrodeposited film. For a given degree of grid coverage, the secondary c.d.d. can be computed numerically with the approach developed in ref. [92]. During the initial stages, globally the c.d.d. has a space dependence similar to the final one, onto which a fine structure is superimposed, controlled by the concentration of current lines at the bars. Briefly, as expected from the general theory of c.d.d. (e.g. ref. [93]), the central squares, such as #1, exhibit a lower, more homogeneous c.d.d., while squares closer to the outer rim of the grid (#2, #3) bear higher c.d.s, that can be estimated, in the case of a typical secondary c.d.d. for an electrodeposition process to be ca. 2.5 (#2) and 3 (#3) times that of square #1.

3.2.1.2 Electrodeposition mechanism and conditions - The cycle shown in Figure 1 has been designed in order to: (i) grow a composite consisting in principle of two constituents that are formed anodically (PPy, Mn(III, IV)) and cathodically (Mn(0)) and (ii) avoid the build-up of large monomer concentration gradients at the electrode/electrolyte interface during electropolymerisation, on the one hand and to reduce the stripping of metal particles during the anodic pulses, on the other hand. The success of a similar approach for the growth of metal/PPy nanocomposites has been demonstrated in works recently published in our group.³⁵⁻⁴⁰ The initial step #1 does not lead to faradaic reactions, but it is required to relax the compositional double-layer. During the first anodic pulse #2, electropolymerisation of pyrrole takes place and soluble Mn(II) oxidises to insoluble Mn(III)- and/or Mn(IV)-containing species. Under these plating conditions PPy is nucleated and grows forming homogeneous, compact and highly electronically conducting films.^{27,51,94,95} During the subsequent cathodic pulse #3, Mn(0) can in principle be incorporated into PPy (by reduction of soluble Mn(II) to Mn(0)) while simultaneously the PPy substrate undergoes progressive undoping and anodically formed Mn(III)/Mn(IV) compounds can undergo reduction.

As hinted at in Section 2.2, owing to progressive cathodic PPy undoping, the reduction processes taking place during the cathodic pulse are expected to be self-limiting. The following anodic pulse #4 causes the redoping of the pre-existent PPy film and the oxidation of pre-existent Mn(0) or

Mn(II), together with further Mn(III,IV)/PPy electrodeposition. It is worth noting that, according to thermodynamics in aqueous solution, cathodically formed Mn metal is expected to oxidise under the conditions prevailing during the anodic step of the electrodeposition process and subsequent exposure to air.⁷³ According to the results of Section 3.1.1.3, the optimal pulse sequence is: 0 V 5 s, 1.2 V 0.5 s, -1.8 V, 2 s, 1.2 V 0.5 s. 15 electrodeposition cycles allowed ideal soft X-ray transmission for STXM and XAS measurements.

In this study, we analyse and compare the compositional and chemical-state distribution of composite Mn/PPy films, as a function of local c.d.d.. In particular, we investigated representative areas within the three squares #1, #2 and #3 depicted in Figure 5-A, exhibiting increasing c.d. values.

3.2.1.3 STXM and XRF mapping - In Figures 5 and 6 we report a selection of fluorescence maps, that is representative of the compositional distributions at mesoscopic and submicrometric scales, achieved in the c.d.d. conditions corresponding to the locations #1 (low current density) and #3 (high current density) of Figure 5-A. For our compositional analysis, we selected Mn, O and N: Mn and O are representative of the MnO_x dispersoid while N is diagnostic of the polymer distribution, the C edge not being accessible at TwinMic. The scattering maps (bottom right panels of Figures 5-B and 6), that are sensitive to the local amount of electrodeposited material with limited dependence on the local chemical details, are diagnostic of the growth morphology, while the Mn maps divided by the scattering maps highlight the pure elemental distribution and the rationed Mn/O (bottom left panels) and Mn/N (top right panels) pinpoint the relative elemental distributions. A granular morphology is found in both regions, with co-location of the three analysed elements, denoting the fact that MnO_x and polypyrrole act as nucleation centres for the material electrodeposited in both the anodic or cathodic pulses. This is in agreement with the classical nucleation and growth mechanism for electrodeposition by pulse-plating.⁹⁴ The morphology of the composites is not significantly affected by the local c.d. level, while a slightly higher Mn concentration is found in the

higher-c.d. zone #3, coherently with the electrokinetic analysis of Section 3.1.1.. It is worth noting that the electrodeposit morphology and elemental distribution can be followed accurately with the dynamic morphochemical electrodeposition model expounded in ref.s [51,96]; a dedicated parameter identification study will be published separately.

3.2.1.4 Micro-XAS - Figure 7 reports the micro-XAS Mn L₂ spectra recorded in sample locations at different distances from the centre to the periphery of the TEM grid, which correspond to locations of increasing c.d.. The Mn XAS spectra have distinct features for different Mn oxidation states, some of them being at very close photon energies, so they can overlap in the case of coexistence of several oxidation states.⁹⁷ However, the general trend is that the Mn L₂ XAS spectral features shift towards higher photon energies with increasing oxidation state. Comparing the spectra displayed in Figure 7, one can clearly see that they vary in intensity and lineshape with position, which indicates that differences in c.d. induce inhomogeneities both in the amount and in the chemical state of electrodeposited Mn. Also, none of the spectra exhibits the pure lineshape of a single Mn oxidation state, but typically consist of two or three overlapping components. Moving from lower to higher c.d.s there is a systematic spectral shift to higher photon energies, indicative of the fact that higher c.d.s favour the deposition of more oxidised forms of Mn.

3.3 In situ SPEM study of the pyrolysis of Mn/PPy composites

Since the structural and chemical details of the surface are crucial for the catalyst performance, we used in situ SPEM to explore the evolution of the morphology and of the chemical state of the Mn centres resulting from the pyrolysis process. In particular, we performed two in situ annealing steps at 400 and 670°C. Figure 8 shows three Mn 3p SPEM maps of an Mn/PPy electrodeposit grown with 60 pulse-plating cycles (see Section 3.1.1.3), identified as the optimal number by gauging the catalytic performance of the pyrolysed material according to the protocol devised in ref. [57]. Panels (A), (B) and (C) correspond to the pristine sample at room temperature and after annealing at

400°C for 7 h and at 670 °C for 10 h, respectively. The contrast of the maps provides clear evidence of the fact that Mn - as sampled with the utmost surface sensitivity that is typical of photoelectron spectroscopy, of course very different from that of XAS and XRF - is uniformly distributed in the pristine sample, while annealing creates inhomogeneity in the Mn distribution. The final morphology observed by SPEM during in situ pyrolysis closely matches the typical SEM topography obtained by pyrolysis in an oven (Panel (D)).

Figure 9 (Panels (a) and (b)) shows the evolution of Mn 2p_{3/2} and Mn 3p spectra recorded at representative times of the above-specified annealing protocol. These spectra were taken in the microspot mode in random positions of the pristine sample (Figure 8-A) and on the Mn grains imaged in Panels (B) and (C) of Figure 8. The binding energies corresponding to the different Mn oxidation states are indicated in the Panels and for the sake of comparison the Mn 2p_{3/2} and 3p spectra of metallic Mn, measured on a freshly sputtered, atomically clean Mn sample are plotted as well.⁹⁸⁻¹⁰⁵ The lineshapes of both the Mn 2p_{3/2} and Mn 3p spectra indicate the coexistence of typically three Mn oxidation states. It is worth noting that the Mn 2p_{3/2} and Mn 3p spectra of the pristine sample exhibit different amounts of the Mn⁰, Mn²⁺ and Mn³⁺ components. This difference is typical of core-shell structures and results from the different escape depths of Mn 2p_{3/2} and 3p photoelectrons (~5 and ~10 Å, respectively). In our case the pristine sample is found to exhibit an oxidised top surface layer (dominated by the Mn 2p_{3/2} signal), whereas the subsurface layers (probed preferentially by the Mn 3p spectra) contain a higher fraction of the metallic component and the +2 oxidation state appears dominant. As a result of this particular structure of the starting material, only minor differences - essentially only a weak increase of the Mn⁴⁺ component - are found in the Mn 2p_{3/2} spectra between the pristine and pyrolysed conditions. On the contrary, the Mn 3p spectra are very sensitive to the progress of pyrolysis, that brings about a notable, progressive increase in the intensity of the Mn³⁺ and Mn⁴⁺ components.¹⁰¹ Relevant Mn redox chemistry – the details of which are beyond the scope of the present paper – are compatible with a scenario

implying hydrogen abstraction from Mn(II) hydroxide (see, e.g. ref.s [106-108]). The presence of mixed Mn^{3+/4+} oxides is desirable for ORR electrocatalysis since the role of the catalyst is to provide an adsorption site for molecular oxygen, that will drive its subsequent reduction. In principle, the two prototypical cases of molecular oxygen adsorption are the merely reductive type, resulting in the 2e⁻ mechanism, that is typical of MnO_x (Eq. 7) and the dissociative and reductive type, leading to 4e⁻ reduction, that is typical of CoO_x.¹⁰⁹



The N 1s micro-XPS spectra measured during pyrolysis are shown in Panel (c) of Figure 9. The different spectral features match those reported in the literature for metal/nitrogen/carbon ORR catalysts, that correspond to four types of N-functionalities: (i) pyridinic N and (ii) metal-bonded N at 397-399.5 eV; (iii) pyrrolic N at 399.9-400.7 eV, and (iv) graphitic N at 401-403 eV^{42,110,111}. In particular, feature (ii) has been assigned to metal-nitrogen bonds on the surface of the catalyst.^{6,112,113} The N 1s spectra measured in situ were deconvoluted using these four components. The pristine sample shows a broad peak with three components: the most intense peak at 399.7 eV corresponds to N-pyrrolic, the shoulder at 398.2 eV indicates the presence of pyridinic or metal-bonded nitrogen, and the other shoulder at ca. 402 eV is a contribution of polaronic defects in the PPy matrix.^{42,114,115} Since the N 1s component at 398.2 eV is absent in the XPS spectrum of pure PPy,¹¹⁴ our results suggest that the chemical state of N of pure PPy is modified by the presence of Mn in the polymer structure, coherently with the outcomes of our SERS measurements (Section 3.1.2). With increasing temperature, a gradual change of the N 1s signal is observed in agreement with literature data on pyrolysed PPy-based materials.^{42,116-119} Such evolution of the N 1s XPS

features is related to the thermal decomposition of PPy, that is reported to begin at ca. 300°C,¹¹⁷ where on the one hand the cracking of the pyrrolic rings generates polymer fragments such that pyrrolic-N becomes pyridinic-N and/or graphitic N and on the other hand volatile species are formed.^{120,121} The intensity of the N-pyrrolic component decreases, while that of the graphitic and pyridinic/Mn-N features increases; it is worth noting that the species that were found to form are those reported to exhibit higher ORR catalytic activity.¹²²⁻¹²⁵ The permanence of a weak N-pyrrolic feature after prolonged heat treatment at 670°C suggests that PPy has not been totally pyrolysed: this result is compatible with recent XRD analyses, showing that PPy reaches a complete carbonisation only at temperatures higher than 800 °C.¹²⁶

4. CONCLUSIONS

In this paper we investigated the electrodeposition of Mn/PPy composites and their pyrolysis treatment, in view of improving their electrocatalytic ORR activity and durability. As highlighted by cyclic voltammetric analyses, in-situ micro Raman spectroscopy and micro-XAS, the potentiostatic pulsed co-deposition process - alternating anodic and cathodic polarisation intervals -, leads to a PPy deposit containing manganese (II, III, IV) oxy-hydroxides and traces of Mn(0). XRF mapping of codeposits discloses a rather homogeneous Mn distribution and local XAS reveals that the relative amounts of Mn(II), Mn(III) and Mn(IV) follow, though with slight changes, the local c.d.d., with higher valences dominating in the high-c.d. zones. The pyrolysis process has been monitored in situ by micro-XPS: Mn, initially present in a core-shell structure with a metallic core and a Mn(II,III) shell, tends to oxidise achieving a final composition in which Mn(III) and Mn(IV) dominate; the partial decomposition of Mn/PPy results in a rearrangement of the chemical structure of PPy with the formation of novel Me-N bonds and graphitic-N functionalities, that can be regarded as the active sites of this class of electrocatalysts. As reported in ref. [40], the pyrolysed material exhibits a notably better durability under ORR conditions than in the as-electrodeposited

form. As far as the electrocatalytic performance is concerned, the onset and halfwave potentials for the pyrolysed material are shifted with respect to the values measured for the corresponding as-electrodeposited system, denoting considerably improved activity. In terms of the same electrocatalytic figures of merit, our electrocatalyst outperforms MnO_x supported on a range of carbons, such as: C-powders,¹²⁷ vulcan,^{31,128} and nanocarbon,¹²⁹ while mesoporous C-N supports¹³⁰ and appropriately nanostructured MnO_2 (nanospheres and nanowires,¹³¹ microsphere/nanosheet core–corona hierarchical architectures, nanorods, and nanotubes¹³²) yield better ORR capabilities.

FIGURE CAPTIONS

Figure 1 – (Top) Potentiostatic square-wave sequence employed for the pulse-plating of the Mn/PPy composites and (bottom) a selection of representative current density transients resulting from the application of the potentiostatic pulse sequence.

Figure 2 - Cyclic voltammograms corresponding to: (A) pyrrole polymerisation, (B) Mn electrodeposition and (C) codeposition of polypyrrole and Mn. GC electrode in contact with acetonitrile / water 1 vol.% solutions containing 0.1 M TBAP, with added: (A) 0.1 M pyrrole; (B) 0.05 M MnCl₂ and (C) 0.1 M pyrrole and 0.05 M MnCl₂. Scan rate 0.1 V s⁻¹.

Figure 3 - FE-SEM micrographs of pyrolysed Mn/PPy deposits as a function of the number of pulse-plating cycles, as indicated. A typical EDX spectrum recorded in a typical area containing Mn grains is overlapped to the top-right image.

Figure 4 - Potential-dependent in situ Raman spectra recorded in acetonitrile / water 1 vol.% solutions containing 0.1 M TBAP, with added: (A) 0.05 M MnCl₂ and (B, C) 0.1 M pyrrole and 0.05 M MnCl₂. The spectra for doped and undoped states, denoted by a star are reproduced from ref. [39].

Figure 5 – (A) Scheme of the locations of the Mn/PPy-coated TEM grid used as working electrode for STXM, XRF mapping and micro-XAS. (B) XRF maps (scattering and ratiomed Mn/scattering Mn/N and Mn/O) of the Mn/PPy film grown in square #1 (low current density region) of Panel (A) (acquired at 785 eV with 250 nm spot size).

Figure 6 – XRF maps (scattering and ratiomed Mn/scattering Mn/N and Mn/O) of the Mn/PPy film grown in square #3 (high current density region) of Figure 5-A (acquired at 785 eV with 250 nm spot size).

Figure 7 – Micro-XAS spectra at the Mn L₂ edge, recorded in positions corresponding to representative distances from the centre of the TEM grid. The top spectrum was measured with an MnO standard. The vertical lines indicate the position of the most intense feature for the different Mn oxidations states.

Figure 8 – (A)-(C) SPEM images at Mn 3p energy of Mn/PPy (60 pulse-plating cycles) subjected to in situ pyrolysis. (A) Pristine sample, room temperature; (B) same sample at 400°C, after 7 h of annealing at this temperature; (C) same sample at 670°C, after 10 h of annealing at this temperature; (D) SEM of a similar sample after pyrolysis in oven.

Figure 9 – Micro-XPS spectra measured during in situ pyrolysis of Mn/PPy (60 pulse-plating cycles) at the following core levels: (a) Mn 2p_{3/2}, (b) Mn 3p (c) N 1s. (A) For Mn: metallic Mn reference, for N a pure polypyrrole sample reproduced from the literature¹¹⁴; (B) pristine electrodeposit; (C) at 400°C, after 7 h of heat treatment at this temperature; (D) at 670°C, after 10 h of heat treatment at this temperature; (E) at the end of the whole pyrolysis protocol, after cooling down to room temperature.

REFERENCES

- [1] S. Srinivasan, *J. Electrochem. Soc.*, 1989, **136**, C41.
- [2] C. Chakkaravarth, A. K. Abdul Waheed and H. V. K. Udupa, *J. Power Sources*, 1081, **6**, 203.
- [3] R. Jasinski, *Nature*, 1964, **201**, 1212.
- [4] V. S. Bagotzky, M. R. Tarasevich, K. A. Radyushkina, O. A. Levina and S. I. Andrusyova, *J. Power Sources*, 1978, **2**, 233.
- [5] A. Van Der Putten, A. Elzing, W. Visscher and E. Barendrecht, *J. Electroanal. Chem. Interf. Electrochem.*, 1986, **205**, 233.
- [6] G. Faubert, G. Lalande, R. Cote, D. Guay, J. P. Dodelet, L. T. Weng, P. Bertrand and G. Denes, *Electrochim. Acta*, 1996, **41**, 1689.
- [7] E. Yeager, *Electrochim. Acta*, 1984, **29**, 1527.
- [8] K. Wiesener, *Electrochim. Acta*, 1986, **31**, 1073.
- [9] S. Ye and A. K. Vijh, *Int. J. Hydrogen Energy*, 2005, **30**, 1011.
- [10] H. J. Zhang, X. Yuan, L. Sun, X. Zeng, Q. Z. Jiang, Z. Shao and Z. F. Ma, *Int. J. Hydrogen Energy*, 2010, **35**, 2900.
- [11] Y. Ji, Z. Li, S. Wang, G. Xu and X. Yu, *Int. J. Hydrogen Energy*, 2010, **35**, 8117.
- [12] Y. Ichiro, R. Ichihashi, T. Iwasaki, N. Nishimura, T. Murayam, W. Ueda and S. Takenaka, *Electrochim. Acta*, 2013, **108**, 321.
- [13] R. Jiang and D. Chu, *J. Power Sources*, 2014, **245**, 352.
- [14] M. Lefevre, E. Proietti, F. Jaouen and J.P. Dodelet, *Science*, 2009, **324**, 71.
- [15] S. Gupta, D. Tryk, I. Bae, W. Aldred and E. Yeager, *J. Appl. Electrochem.*, 1989, **19**, 19.
- [16] P. H. Matter and U. S. Ozkan, *Catal. Lett.*, 2006, **109**, 115.
- [17] P. H. Matter, L. Zhang and U. S. Ozkan, *J. Catal.*, 2006, **239**, 83.
- [18] P. H. Matter, E. Wang, J. M. M. Millet and U.S. Ozkan, *J. Phys. Chem. C*, 2007, **111**, 1444.
- [19] R. A. Sidik, A. B. Anderson, N. P. Subramanian, S. P. Kumaraguru and B. N. Popov, *J. Phys. Chem. C*, 2006, **110**, 1787.
- [20] C. W. B. Bezerra, L. Zhang, K. C. Lee, H. S. Liu, J. L. Zhang, Z. Shi, A. L. B. Marques, E. P. Marques, S. H. Wu and J. J. Zhang, *Electrochim. Acta*, 2008, **53**, 7703.
- [21] U.I. Kramm, I. Herrmann-Geppert, P. Bogdanoff and S. Fiechter, *J. Phys. Chem. C*, 2011, **115**, 23417.
- [22] B. Wang, *J. Power Sources*, 2005, **152**, 1.
- [23] D. Villers, X. Jacques-Bedard and J. P. Dodelet, *J. Electrochem. Soc.*, 2004, **151**, A1507–A1515.
- [24] C. Medard, M. Lefevre, J. P. Dodelet, F. Jaouen and G. Lindbergh, *Electrochim. Acta*, 2006, **51**, 3202.
- [25] J. A. R. van Veen, H. A. Colijn and J. F. van Baar, *Electrochim. Acta*, 1988, **33**, 801.
- [26] H. V. Rasika Dias, M. Fianchini and R. M. Gamini Rajapakse, *Polymer*, 2006, **47**, 7349.
- [27] S. Sadki, P. Schottland, N. Brodie and G. Sabouraud, *Chem. Soc. Rev.*, 2000, **29**, 283.
- [28] H. Nguyen-Cong, K. El-Abbassi, J. L. Gautier and P. Chartier, *Electrochim. Acta*, 2005, **50**, 1369.
- [29] A. Deronzier and J. C. Moutet, *Coord. Chem. Rev.*, 1996, **147**, 339.
- [30] E. Simon, E. Sable, H. Handel and M. L'Her, *Electrochim. Acta*, 1999, **45**, 855.
- [31] J. Vondrák, B. Klápšte, J. Velická, M. Sedlaříková, V. Novák and J. Reiter, *J. New Mater. Electrochem. Syst.*, 2005, **8**, 209.
- [32] J. Vondrák, B. Klápšte, J. Velická, M. Sedlaříková, V. Novák and J. Reiter, *J. New Mater. Electrochem. Syst.*, 2005, **8**, 1.
- [33] L. Mao, D. Zhang, T. Sotomura, K. Nakatsu, N. Koshiba and T. Ohsaka, *Electrochim. Acta*, 2003, **48**, 1015.
- [34] J. Masa, T. Schilling, M. Bron and W. Schuhmann, *Electrochim. Acta* 2012, **60**, 410.
- [35] B. Bozzini, A. Gianoncelli, P. Bocchetta, S. Dal Zilio and G. Kourousias, *Anal. Chem.*, 2014, **86**, 664.

- [36] B. Bozzini, P. Bocchetta, A. Gianoncelli, C. Mele and M. Kiskinova, *ChemElectroChem*, DOI: 10.1002/celec.201500138.
- [37] B. Bozzini, P. Bocchetta, A. Gianoncelli, G. Kourousias, S. Dal Zilio and M. Kiskinova, *J. Vac. Sci. Technol. A*, 2015, **33**, 031102.
- [38] B. Bozzini, P. Bocchetta and A. Gianoncelli, *Energies*, 2015, **8**, 8145.
- [39] P. Bocchetta, A. Gianoncelli, M. Abyaneh, M. Kiskinova, M. Amati, L. Gregoratti, D. Jezeršek, C. Mele and B. Bozzini, *Electrochim. Acta*, 2014, **137**, 535.
- [40] P. Bocchetta, M. Amati, L. Gregoratti, M. Kiskinova, H. Sezen, A. Taurino and B. Bozzini, *J. Electroanal. Chem.*, in press.
- [41] J. Cao, X. Li, Y. Wang, F. C. Walsh, J.-H. Ouyang, D. Jia and Y. Zhou, *J. Power Sources*, 2015, **293**, 657.
- [42] K. Lee, L. Zhang, H. Lui, R. Hui, Z. Shi and J. Zhang, *Electrochim. Acta*, 2009, **54**, 4704.
- [43] T. S. Olson, S. Pylypenko, P. Atanassov, K. Asazawa, K. Yamada, and H. Tanaka, *J. Phys. Chem. C*, 2010, **114**, 5049.
- [44] X. Yuan, X. Zeng, H.-J. Zhang, Z.-F. Ma and C.-Y. Wang, *J. Am. Chem. Soc.*, 2010, **132**, 1754.
- [45] H. Y. Qin, Z. X. Liu, Li Q. Ye, J. K. Zhu and Z. P. Li, *J. Power Sources*, 2009, **192**, 385.
- [46] V. Nallathambi, J. W. Lee, S. P. Kumaraguru, G. Wu and B. N. Popov, *J. Power Sources*, 2008, **183**, 34.
- [47] F. Jaouen and J.-P. Dodelet, *J. Phys. Chem. C*, 2009, **113**, 15422.
- [48] H. Ma and B. Wang, *RSC Adv.*, 2014, **4**, 46084.
- [49] A. Zhao, J. Masa, W. Xia, A. Maljusch, M.-G. Willinger, G. Clavel, K. Xie, R. Schlögl, W. Schuhmann and M. Muhler, *J. Am. Chem. Soc.* 2014, **136**, 7551.
- [50] X. Yu and A. Manthiram, *Catal. Sci. Technol.*, 2015, **5**, 2072.
- [51] A. Gianoncelli, I. Sgura, P. Bocchetta, D. Lacitignola and B. Bozzini, *X-RAY Spectrometry*, 2015, **44**, 191.
- [52] B. Bozzini, A. Gianoncelli, B. Kaulich, C. Mele, M. Prasciolu and M. Kiskinova, *J. Power Sources*, 2012, **211**, 71.
- [53] T. Rapecki, M. Donten and Z. Stojek, *Electrochem. Comm.*, 2010, **12**, 624.
- [54] Y. Haseko, N. K. Shrestha, S. Teruyama, and T. Saji, *Electrochim. Acta*, 2006, **51**, 3652.
- [55] M. Chipara, R. Skomski and D. J. Sellmyer, *Mater. Lett.*, 2007, **61**, 2412.
- [56] R. K. Sharma, A. C. Rastogi and S. B. Desu, *Electrochim. Acta*, 2008, **53**, 7690.
- [57] P. Bocchetta, M. Amati, B. Bozzini, M. Catalano, A. Gianoncelli, L. Gregoratti, A. Taurino and M. Kiskinova, *ACS Appl. Mater. Interfaces*, 2014, **6**, 19621.
- [58] B. Bozzini, P. Bocchetta, A. Gianoncelli, C. Mele and M. Kiskinova, *Acta Chim. Slov.*, 2014, **61**, 263.
- [59] F. Beck, M. Oberst and R. Jansen, *Electrochim. Acta*, 1990, **35**, 1841.
- [60] A. J. Downard and D. Pletcher, *J. Electroanal. Chem.*, 1986, **206**, 139.
- [61] M. Zhou and J. Heinze, *J. Phys. Chem. B*, 1999, **103**, 8451.
- [62] N. V. Kaminskaia and N. M. Kostic, *J. Chem. Soc., Dalton Trans.*, 1966, 3677.
- [63] C. Mele and B. Bozzini, *J. Solid State Electrochem.*, 2009, **13**, 1553.
- [64] T. F. Otero and I. Boyano, *J. Phys. Chem. B*, 2003, **107**, 6730.
- [65] F. C. Walsh and C. Ponce de León, *Surf. Coat. Technol.*, 2014, **259**, 676.
- [66] T. F. Otero, S. O. Costa, M. J. Ariza and M. Marquez, *J. Mater. Chem.*, 2005, **15**, 1662.
- [67] S. Günther, B. Kaulich, L. Gregoratti and M. Kiskinova, *Progr. Surf. Sci.*, 2002, **70**, 187.
- [68] A. W. Potts, G. R. Morrison, L. Gregoratti, A. Barinov, B. Kaulich and M. Kiskinova, *Surf. Rev. Lett.*, 2002, **9**, 705.
- [69] B. Kaulich, J. Susini, C. David, E. Di Fabrizio, G. Morrison, P. Charalambous, J. Thieme, T. Wilhein, J. Kovac, D. Bacescu, M. Salome, O. Dhez, T. Weitkamp, S. Cabrini, D. Cojoc, A. Gianoncelli, U. Vogt, M. Podnar, M. Zangrando, M. Zacchigna, and M. Kiskinova, *Proc. 8th Int.*

- Conf. X-ray Microscopy*, S. Aoki, Y. Kagoshima, Y. Suzuki, Eds., Conf. Proc. Series IPAP: Tokyo, Japan, 2005, Volume 7, pp. 22-25.
- [70] B. Kaulich, P. Thibault, A. Gianoncelli and M. Kiskinova, *J. Phys. Condensed Matter.*, 2011, **23**, 083002.
- [71] F. Trinidad, J. Alonso-Lopez and M. Nebot, *J. Appl. Electrochem.*, 1987, **17**, 215.
- [72] M. Zhou and J. Heinze, *Electrochim. Acta*, 1999, **44**, 1733.
- [73] M. Pourbaix, *Atlas of Electrochemical Equilibria in Aqueous Solutions*, National Association of Corrosion Engineers, Houston, TX, 1966.
- [74] B. Messaoudi, S. Joiret, M. Keddami and H. Takenouti, *Electrochim. Acta*, 2001, **46**, 2487.
- [75] S. Rodrigues, A. K. Shukla, N. Munichandraiah, *J. Appl. Electrochem.*, 1998, **28**, 1235.
- [76] J. P. Petitpierre, C. Comninellis and E. Plattner, *Electrochim. Acta*, 1990, **35**, 281.
- [77] A. Manivel, N. Ilayaraja, D. Velayutham and M. Noel, *Electrochim. Acta*, 2007, **52**, 7841.
- [78] M. M. Morrison and D. T. Sawyer, *Inorg. Chem.*, 1978, **17**, 333.
- [79] Suhasini, *J. Electroanal. Chem.*, 2013, **690**, 13.
- [80] P. Radhakrishnamurthy and A. K. N. Reddy, *J. Appl. Electrochem.*, 1974, **4**, 317.
- [81] I. M. Kolthoff and J. F. Coetzee, *J. Am. Chem. Soc.*, 1957, **79**, 1852.
- [82] L. Peng, C. Yao, W. Zhang, Q. Yang, G. Li, Y. Tong and G. A. Hope, *Thin Solid Films* 2008, **516**, 3935.
- [83] S. Devaraj and N. Munichandraiah, *Electrochem. Solid-State Lett.*, 2009, **12**, F21.
- [84] B. Bozzini, E. Tondo, P. Raffa and M. Boniardi, *Trans. IMF*, 2012, **90**, 30.
- [85] M. Sun, B. Lan, L. Yun, F. Ye, W. Song, J. He, G. Diao and Y. Zheng, *Mater. Lett.*, 2012, **86**, 18.
- [86] R. Baddour-Hadjean and J.-P. Pereira-Ramos, *Chem. Rev.*, 2010, **110**, 1278.
- [87] Y. C. Liu and B. J. Hwang, *Thin Solid Films*, 1999, **339**, 233.
- [88] Y.-C. Liu, B.-J. Hwang, W.-J. Jian and R. Santhanam, *Thin Solid Films*, 2000, **374**, 85.
- [89] J. Duchet, R. Legras and S. Demoustier-Champagne, *Synth. Met.*, 1998, **98**, 113.
- [90] A. B. Goncalves, A. S. Mangrich and A. J. G. Zarbin, *Synth. Met.*, 2000, **114**, 119.
- [91] Z. W. Tian, *J. Phys. Chem.*, 1990, **94**, 2171.
- [92] B. Bozzini and I. Sgura, *SIAM J. Appl. Mathem.*, 2009, **70**, 579.
- [93] J. S. Newman, *Electrochemical Systems*, Prentice Hall, Englewood Cliffs (NJ), 1991, Chap. 18.
- [94] K. I. Popov, S. S. Djokic and B. N. Grgur, *Fundamental Aspects of Electrometallurgy*, Kluwer, N.Y., 2002, Chapt. 5, pp. 145-174.
- [95] T. Hernandez-Pérez, M. Morales, N. Batina and M. Salmón, *J. Electrochem. Soc.*, 2001, **148**, C369.
- [96] B. Bozzini, D. Lacitignola and I. Sgura, *J. Solid State Electrochem.*, 2013, **17**, 467.
- [97] B. Gilbert, B. H. Frazer, A. Belz, P. G. Conrad, K. H. Neilson, D. Haskel, J. C. Lang, G. Srajer, and G. De Stasio, *J. Phys. Chem. A*, 2003, **107**, 2839.
- [98] B. R. Strohmeyer and D. H. Hercules, *J. Phys. Chem.*, 1984, **88**, 4922.
- [99] V. Di Castro and G. Polzonetti, *J. Electron. Spectrosc. Relat. Phenom.*, 1989, **48**, 117.
- [100] B. H. Olesen, R. Avci and Z. Lewandowski, *Corros. Sci.*, 2000, **42**, 211.
- [101] A. J. Nelson, J. G. Reynolds and J. W. Roos, *J. Vac. Sci. Technol. A*, 2000, **18**, 1072 .
- [102] A. A. Audi and P. M. A. Sherwood, *Surf. Interface Anal.*, 2002, **33**, 274.
- [103] M. C. Biesinger, B. P. Payne, A. P. Grosvenor, L. W. M. Lau, A. R. Gerson and R. S. C. Smart, *Appl. Surf. Sci.*, 2011, **257**, 2717.
- [104] J. M. Cerrato, W. R. Knocke, M. F. Hochella, A. M. Dietrich, A. Jones and T. F. Cromer, *Environ. Sci. Technol.*, 2011, **45**, 10068.
- [105] Y. Gorlin, B. Lassalle-Kaiser, J. D. Benck, S. Gul, S. M. Webb, V. K. Yachandra, J. Yano and T. F. Jaramillo, *J. Am. Chem. Soc.*, 2013, **135**, 8525.
- [106] C. R. Goldsmith, A. P. Cole, T. D. P. Stark, *J. Am. Chem. Soc.*, 2005, **127**, 9904.

- [107] G. Yin, A. M. Danby, D. Kitko, J. D. Carter, W. M. Scheper and D. H. Busch, *J Am Chem Soc.*, 2008, **130**, 16245.
- [108] G. Yin, *Acc. Chem Res.*, 2013, **46**, 483.
- [109] A. C. Queiroz and F. H. B. Lima, *J. Electroanal. Chem.*, 2013, **707**, 142.
- [110] R. Arrigo, M. Hävecker, S. Wrabetz, R. Blume, M. Lerch, J. McGregor, E. Parrott, J. Zeitler, L. Gladden, A. Knop-Gericke, R. Schlögl and D.S. Su, *J. Am. Chem. Soc.*, 2010, **132**, 9616.
- [111] J.-Y. Choi, R. S. Hsu and Z. Chen, *J. Phys. Chem. C*, 2010, **114**, 8048.
- [112] T. Okada, M. Gokita, M. Yuasa and I. Sekine, *J. Electrochem. Soc.*, 1998, **145**, 815.
- [113] S. Pylypenko, S. Mukherjee, T. S. Olson and P. Atanassov, *Electrochim. Acta*, 2008, **53**, 7875.
- [114] L. Atanasoska, K. Naoit and W. H. Smyrl, *Chem. Mater.*, 1992, **4**, 988.
- [115] A. Morozan, P. Jégou, S. Campidelli, S. Palacin and B. Josselme, *Chem. Commun.*, 2012, **48**, 4627.
- [116] L. Zhang, H. Lui, R. Hui, Z. Shi and J. Zhang, *Electrochim. Acta*, 2009, **54**, 4704.
- [117] Z. Lin, G. H. Waller, Y. Liu, M. Liu and C.-P. Wong, *Nano Energy* 2013, **2**, 241.
- [118] X. Zhou, J. Tang, J. Yang, J. Xie and B. Huang, *J. Mater. Chem. A*, 2013, **1**, 5037.
- [119] L. F. Chen, X. D. Zhang, H. W. Liang, M. Kong, Q. F. Guan, P. Chen, Z. Y. Wu and S. H. Yu, *ACS Nano*, 2012, **6**, 7092.
- [120] T. Uyar, L. Toppare and J. Hacaloğlu, *J. Anal. Appl. Pyrolysis* 2002, **64**, 1.
- [121] X. Hong, L. Zhang, T. Zhang, X. Hong, L. Zhang, T. Zhang and F. Qi, *J. Phys. Chem. A*, 2009, **113**, 5397.
- [122] S. Maldonado and K. J. Stevenson, *J. Phys. Chem. B*, 2004, **108**, 11375.
- [123] S. Y. Kim, J. Lee, C. W. Na, J. Park, K. Seo and B. Kim, *Chem. Phys. Lett.*, 2005, **413**, 300.
- [124] J. Ozaki, T. Anahara, N. Kimura and A. Oya, *Carbon*, 2007, **45**, 1847.
- [125] T. Ikeda, M. Boero, S.-F. Huang, K. Terakura, M. Oshima and J. Ozaki, *J. Phys. Chem. C*, 2008, **112**, 14706.
- [126] S. Chao, Z. Lu, Z. Bai, Q. Cui, J. Qiao, Z. Yang and L. Yang, *Int. J. Electrochem. Sci.*, 2013, **8**, 8786.
- [127] A. C. Garcia, F. H. B. Lima, E. A. Ticianelli and M. Chatenet, *J. Power Sources*, 2013, **222**, 305.
- [128] I. Roche and K. Scott, *J. Appl. Electrochem.*, 2009, **39**, 197.
- [129] J. Feng, Y. Liang, H. Wang, Y. Li, B. Zhang, J. Zhou, J. Wang, T. Regier and H. Dai, *Nano Res.*, 2012, **5**, 718.
- [130] Y. Tan, C. Xu, G. Chen, X. Fang, N. Zheng and Q. Xie, *Adv. Funct. Mater.*, 2012, **22**, 4584.
- [131] F. Cheng, Y. Su, J. Liang, Z. Tao and J. Chen, *Chem. Mater.*, 2010, **22**, 898.
- [132] W. Xiao, D. Wang and X. W. Lou, *J. Phys. Chem. C*, 2010, **114**, 1694.

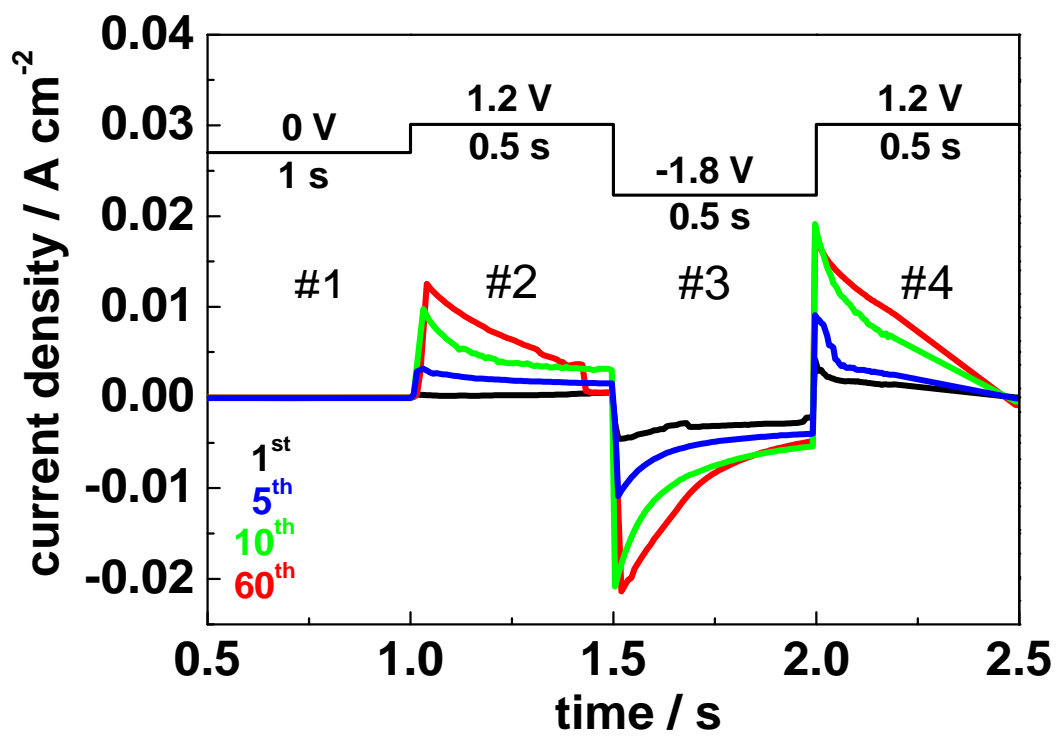


Figure 1

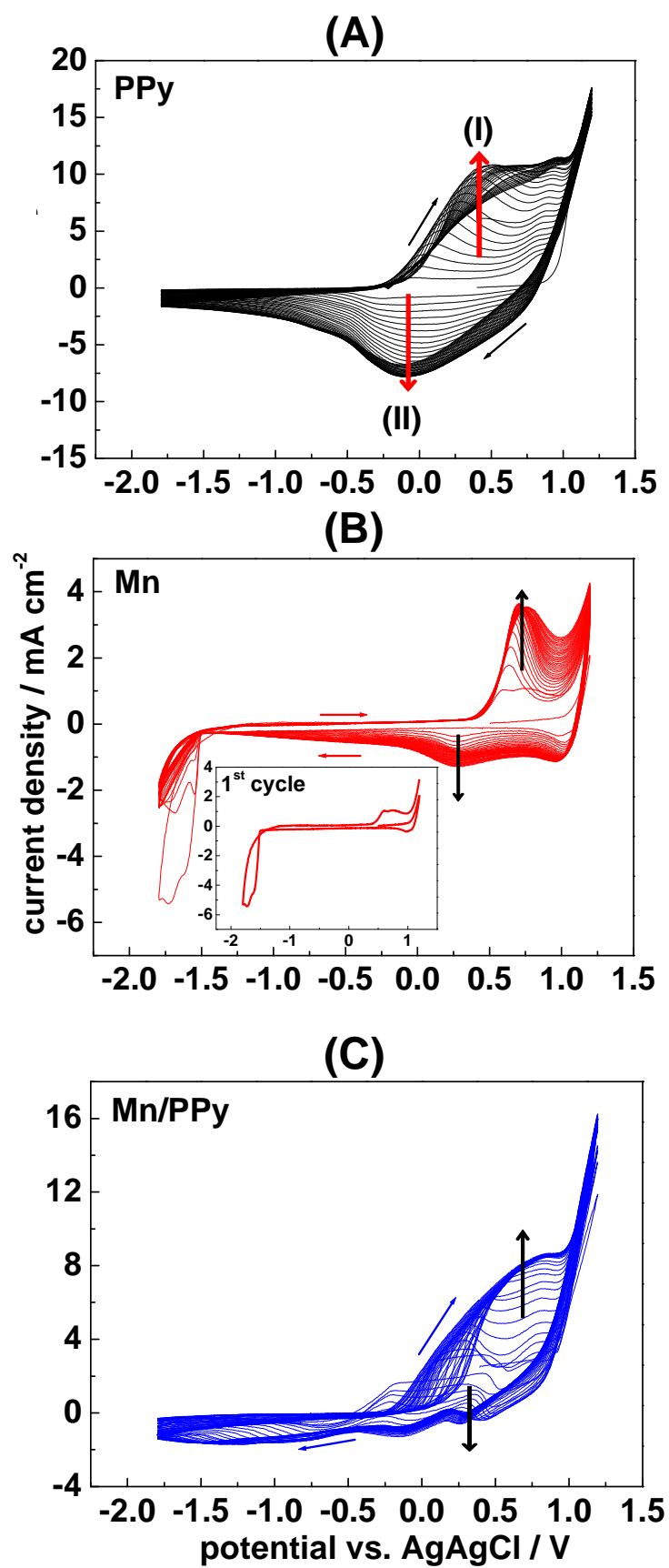


Figure 2

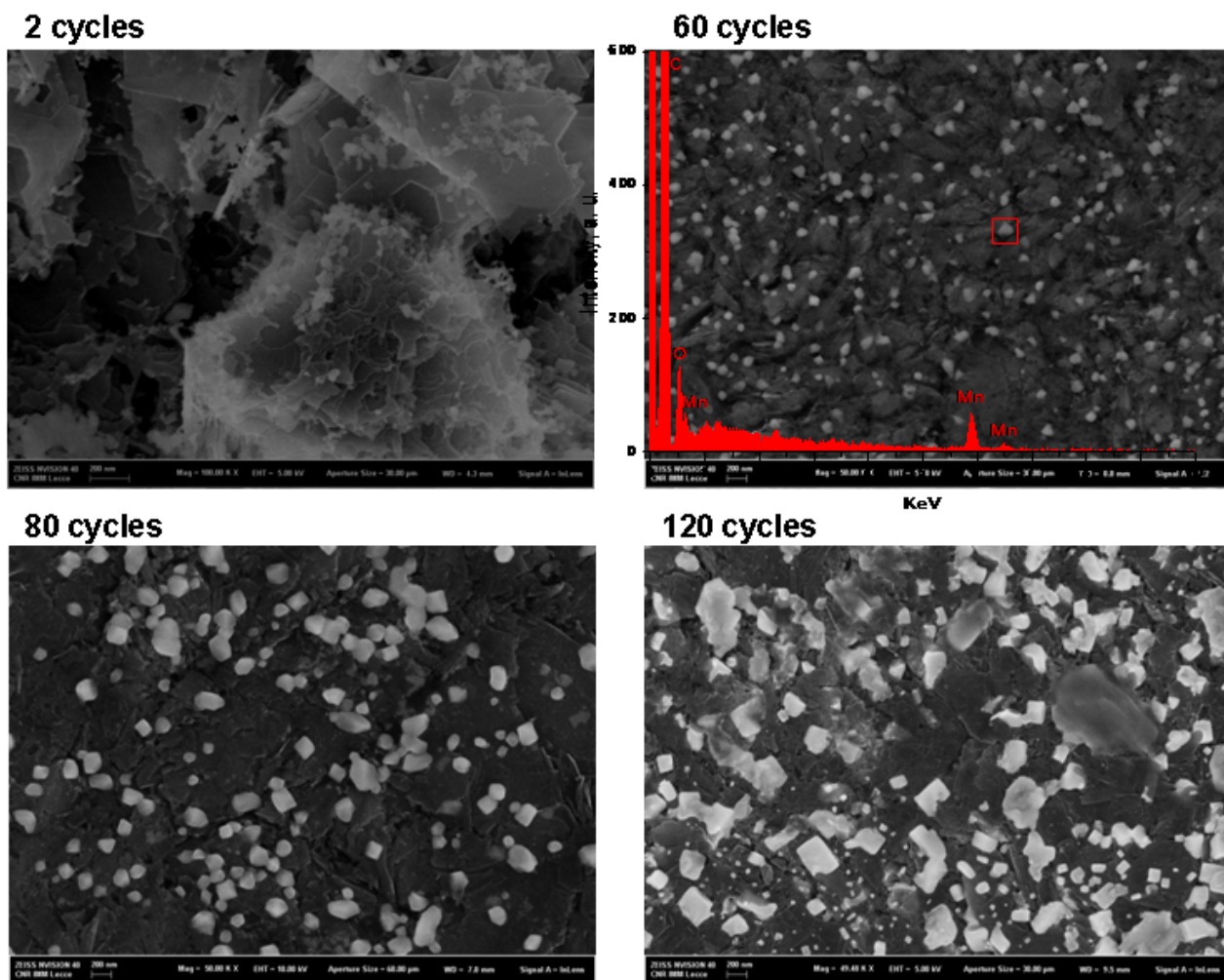


Figure 3

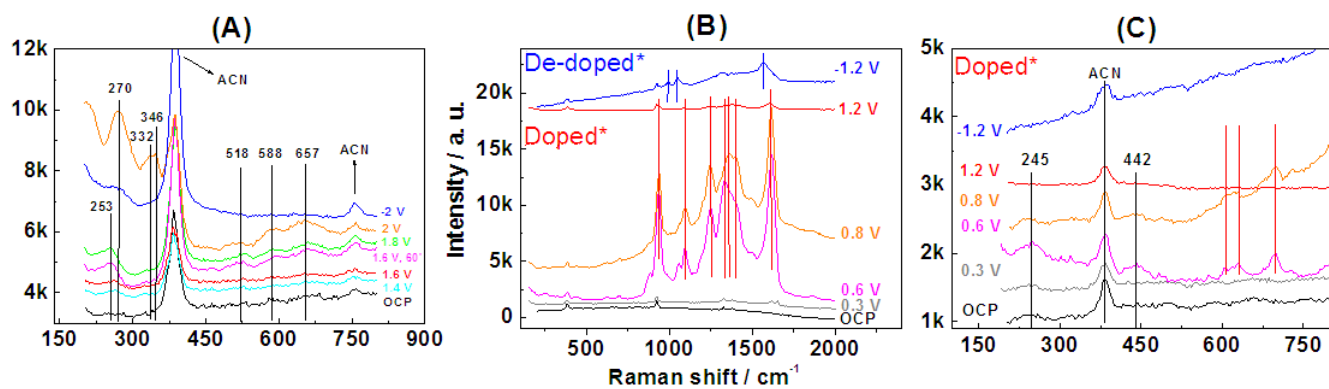


Figure 4

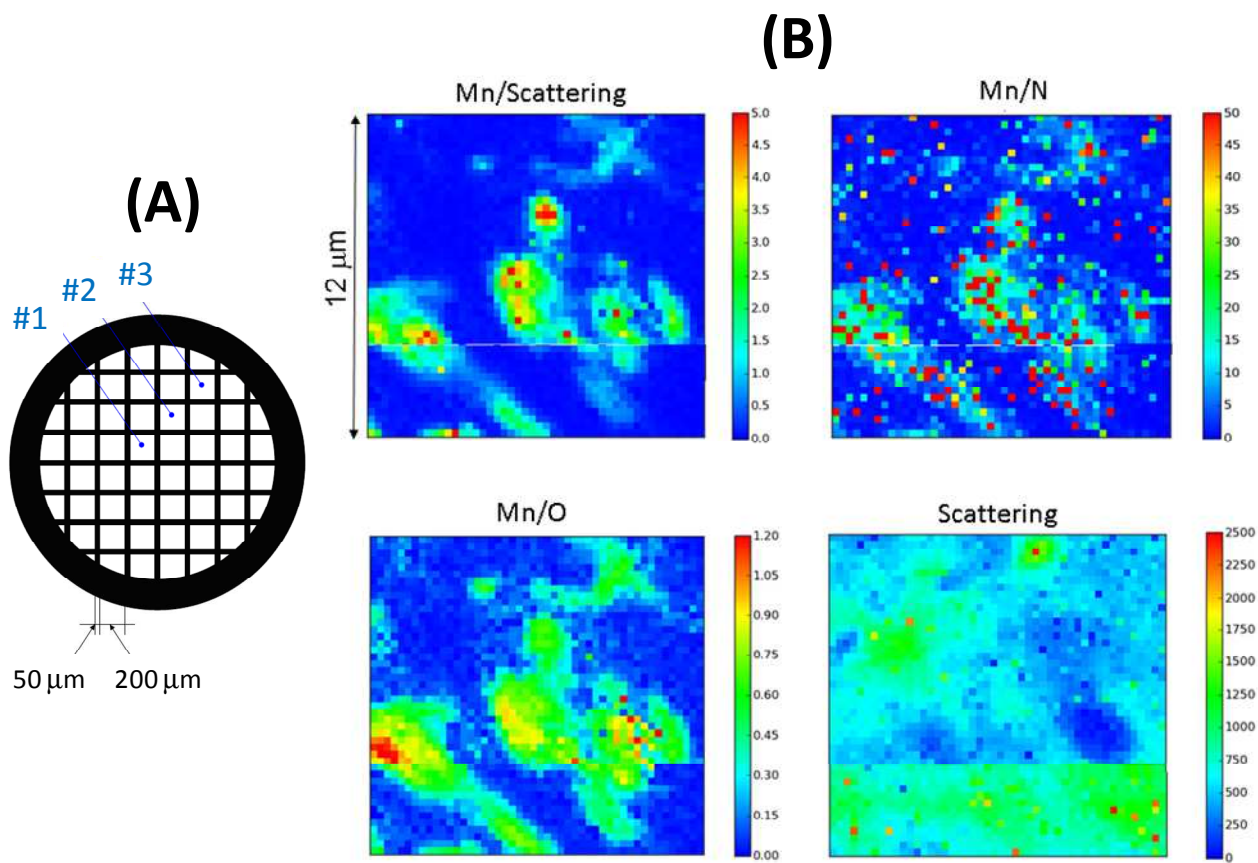


Figure 5

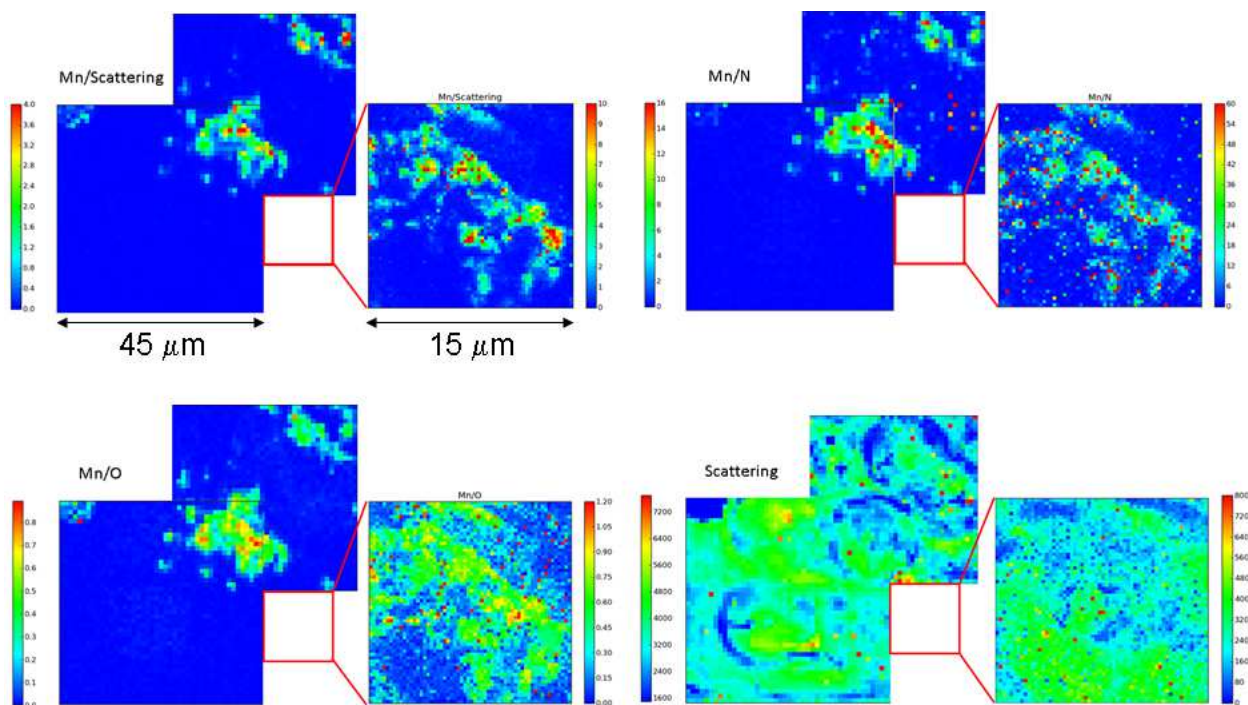


Figure 6

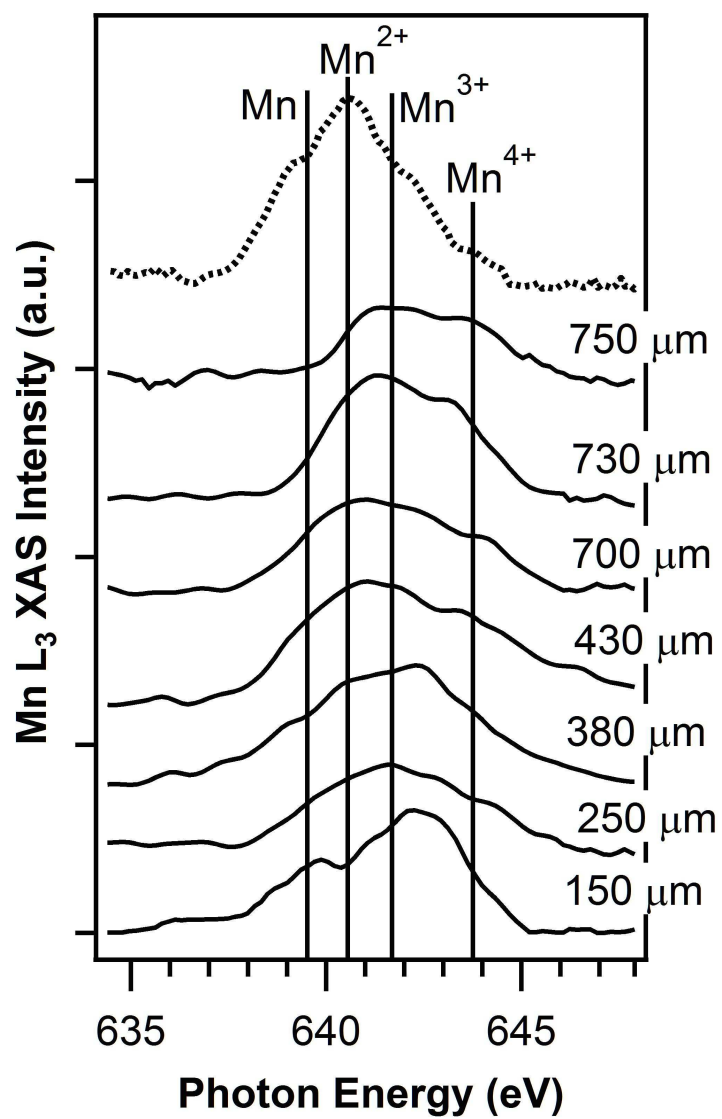


Figure 7

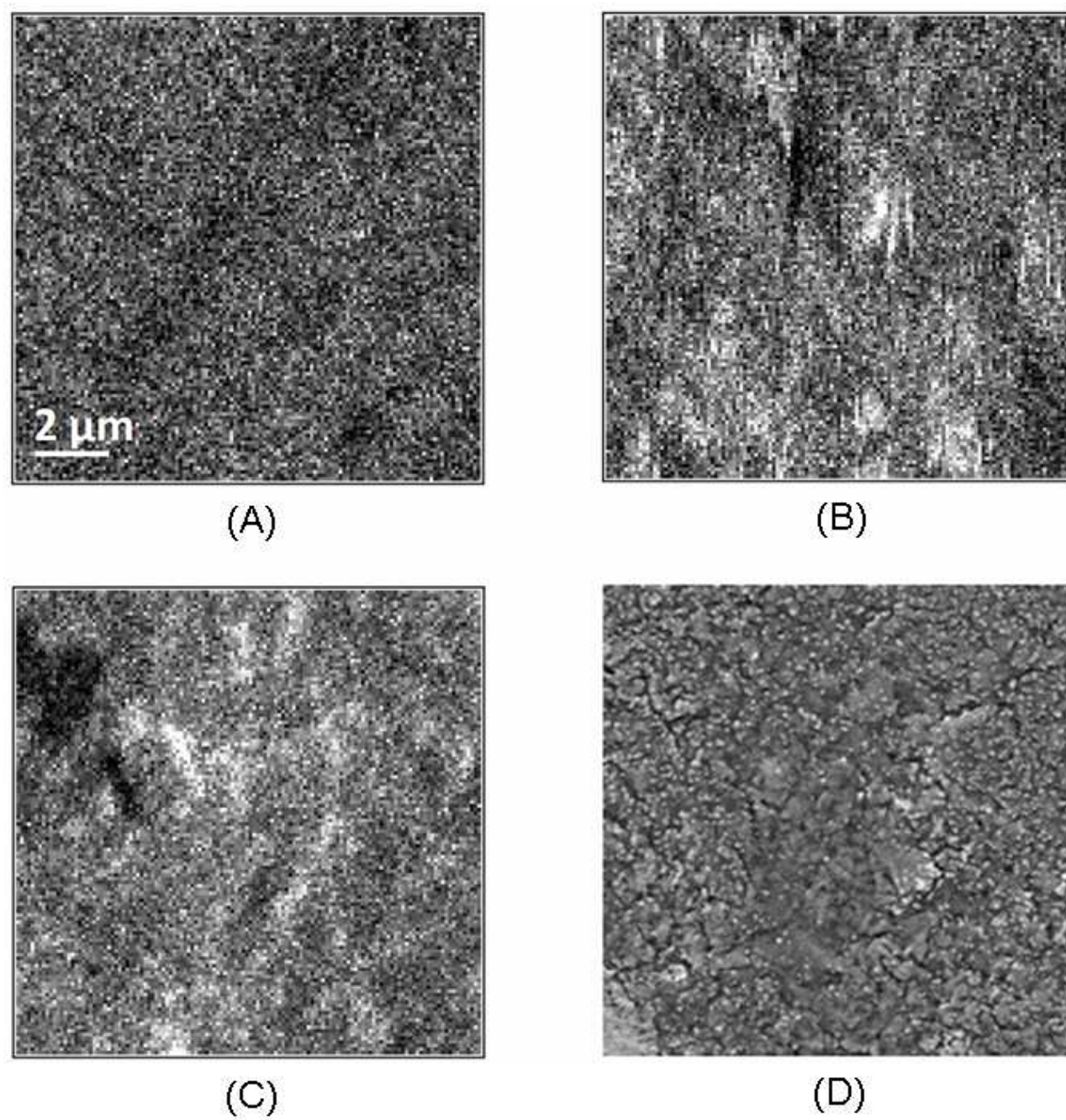


Figure 8

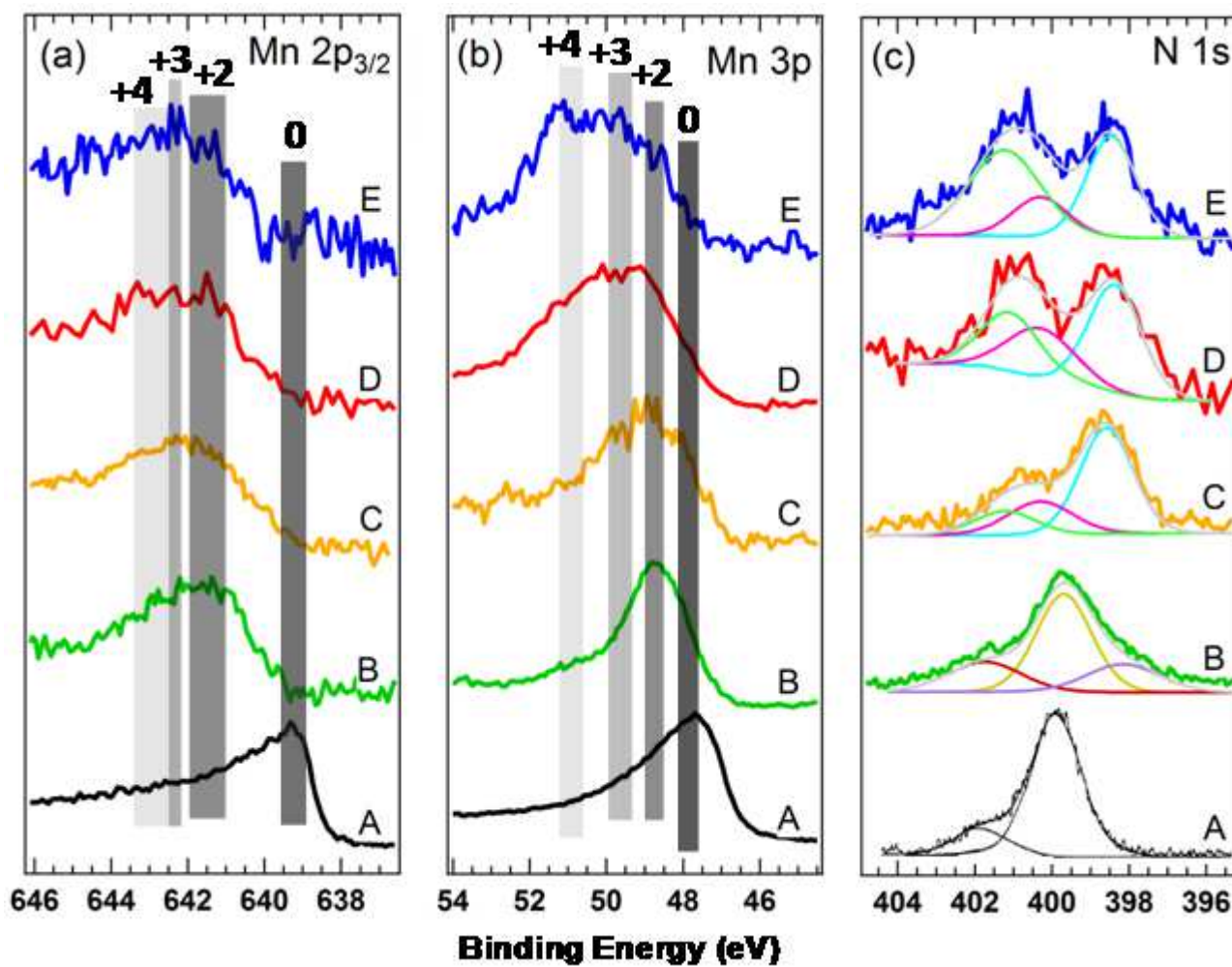


Figure 9

One-pot co-electrodeposition of Mn/polypyrrole composites yields core-shell microparticles, with a partly metallic core, that - as a result of pyrolysis - transform into MnO_x nanoparticles with the desirable blend of oxidation states for ORR electrocatalysis as well as Mn/N/C electroactive sites, exhibiting a combination of graphitic and Mn-bonded N.

